Simulation of plane impinging jets with k-ω based hybrid RANS/LES models

Kubacki S., Dick E.

In: International Journal of Heat and Fluid Flow, 31, 862-878, 2010.

Simulation of plane impinging jets with k-ω based hybrid RANS/LES models

Slawomir Kubacki[a,b], Erik Dick[a,1]
[a]Department of Flow, Heat and Combustion Mechanics, Ghent University,
St.–Pietersnieuwstraat 41, B-9000 Ghent, Belgium
[b]Institute of Aeronautics and Applied Mechanics, Warsaw University of Technology,
Nowowiejska 24, 00-665 Warsaw, Poland

Abstract

Plane impinging jets with nozzle-plate distances H/B=10, 9.2 and 4 and Re=13500, 20000 are simulated with k-ω based hybrid RANS/LES models and with a RANS k-ω model. The results are compared to experimental and LES data. Three different ways of substitution of the turbulent length scale by the local grid size in the LES mode of the hybrid RANS/LES models are tested. The results show that the hybrid models give much better prediction of the wall shear stress and the heat transfer rate along the impingement plate than the pure k-ω RANS model. The good performance of the hybrid models is due to their ability to resolve the evolution and break-up of the vortices in the shear layer of the jet, which strongly affects the turbulent flow and convective heat transfer in the stagnation region and the developing wall-jet region.

Keywords: plane impinging jet, turbulence modelling, k-ω model, hybrid RANS/LES model.

1. Introduction

RANS models present shortcomings for simulation of impinging jet flows such as overestimation of the length of the core region (underestimation of the jet expansion) or overprediction of the turbulent kinetic energy production to dissipation ratio in the stagnation flow region. On the other hand, LES methods are able to reproduce the large scale structures initiated at the jet exit, their evolution and degradation into smaller eddies. However, since LES aims at resolving the scales of motion responsible for turbulence production, it comes into difficulties in near-wall regions, where the size of the eddies is comparable to the Kolmogorov scales, requiring extremely fine grid resolution, approaching that of DNS. In order to alleviate this grid resolution problem in near-wall regions, a hybrid RANS/LES can be applied, where the method acts in RANS mode near walls and in LES mode away from walls.

In the present work, the latest version of the k-ω model of Wilcox (2008) is applied as a "state-of-the-art" turbulence model. Since the RANS model provides poor description of the flow physics for free jet flows, a hybrid RANS/LES model is constructed in order

[1] Corresponding author. Tel.: +32-9-264.33.01; Fax: +32-9-264.35.86. E-mail address: Erik.Dick@UGent.be

to resolve the evolution of the large scale structures in flow regions where the grid density is fine enough, replacing the turbulent length scale by the local grid size. In near wall regions, the model switches to RANS mode, which is known to be adequate for near-wall flows. Three different ways of substitution of the turbulent length scale by the local grid scale are tested.

The first method is based on the concept of Strelets (2001), extending the original DES method by Spalart et al. (1997) to two-equation turbulence models, where the destruction term in the k-equation of the SST k-ω model of Menter (1994) was modified in order to unlock the flow instabilities in regions where the large scale structures are responsible for the major part of the turbulence production. The approach was named Detached Eddy Simulation (DES), according to the principle that the "detached" eddies are simulated while the "attached" eddies (in thin shear layers) are modelled.

The second way of constructing the hybrid RANS/LES approach is according to Davidson and Peng (2003) and Kok et al. (2004), where both the destruction term in the k-equation and the definition for ν_t were modified in such a way that in LES mode the Yoshizawa (1993) model is recovered. The k-ω models used by Davidson and Peng (Peng et al., 1997) and by Kok et al. (Kok, 2000) are own versions with negligible sensitivity to the freestream values of the turbulence variables, in contrast to the original model of Wilcox (1998). A similar concept is used in the latest k-ω model by Wilcox (2008) in order to remove the freestream dependency of the old version (Wilcox, 1998).

The third approach is according to a proposal of Batten et al. (2004), where a latency factor (or latency function) was introduced in the definition of ν_t, based on the ratio of the products of the turbulent length and velocity scales from the underlying RANS and LES models. In the present work, the latency factor is constructed following the work of Sagaut et al. (2006).

Fröhlich and von Terzi (2008) formulated a classification of hybrid RANS/LES models. According to their classification, the hybrid models discussed in the present paper belong to the wide class of interfacing RANS and LES models. Since in LES mode, the local grid size is introduced in place of the turbulent length scale in the destruction term of the k-equation, the first and second models can be further classified as DES type models. The third model belongs to the group called limited numerical scale models (Batten et al., 2004).

Results of simulations of plane impinging jets with nozzle-plate distances H/B=10, 9.2 and 4, and Re=13500, 20000 (Reynolds number based on slot width B and centreline velocity V_0) are presented and compared to experimental data and LES results. The computations have been performed with the FLUENT code version 12, for constant density fluid. The transport equations were implemented with UDFs. We demonstrate that the hybrid RANS/LES models are able to reproduce the evolution of the large scale structures initiated at the jet exit and their break-up into smaller scales. Close to the walls and far away from the free jet flow, the model switches to RANS mode, so that most of the turbulence is modelled there. Overall, good results are obtained.

2. The stress limiter of the k-ω model for hybrid formulation

The continuity and the momentum equations for a constant density fluid are

$$\frac{\partial \overline{u}_i}{\partial x_i} = 0, \tag{1}$$

$$\frac{\partial \overline{u}_i}{\partial t} + \frac{\partial \left(\overline{u}_j \overline{u}_i \right)}{\partial x_j} = -\frac{1}{\rho} \frac{\partial \overline{p}}{\partial x_i} + \frac{\partial}{\partial x_j} \left(\overline{\sigma}_{ji} + \tau_{ji} \right). \tag{2}$$

The overbar in (1) and (2) denotes ensemble averaged quantities in RANS regions and filtered quantities in LES regions. The components of the molecular viscous stress tensor are $\overline{\sigma}_{ij} = 2\nu \overline{S}_{ij}$, with ν the kinematic molecular viscosity and $\overline{S}_{ij} = 1/2 \left(\partial \overline{u}_i / \partial x_j + \partial \overline{u}_j / \partial x_i \right)$ the components of the rate of strain tensor. The components of the modelled stress tensor are $\tau_{ij} = 2\nu_t \overline{S}_{ij} - 2/3 k \delta_{ij}$, where ν_t is the eddy viscosity or the subgrid viscosity.

The latest version of the k-ω model of Wilcox (2008), for a constant density fluid, reads

$$\frac{\partial k}{\partial t} + \frac{\partial \left(\overline{u}_j k \right)}{\partial x_j} = P_k - \beta^* k \omega + \frac{\partial}{\partial x_j} \left[\left(\nu + \sigma^* \frac{k}{\omega} \right) \frac{\partial k}{\partial x_j} \right], \tag{3}$$

$$\frac{\partial \omega}{\partial t} + \frac{\partial \left(\overline{u}_j \omega \right)}{\partial x_j} = \alpha \frac{\omega}{k} P_k - \beta \omega^2 + \frac{\partial}{\partial x_j} \left[\left(\nu + \sigma \frac{k}{\omega} \right) \frac{\partial \omega}{\partial x_j} \right] + \frac{\sigma_d}{\omega} \frac{\partial k}{\partial x_j} \frac{\partial \omega}{\partial x_j}, \tag{4}$$

where k is the turbulent kinetic energy, ω is the specific dissipation rate and $P_k = \tau_{ij} \partial \overline{u}_i / \partial x_j$ is the turbulent kinetic energy production. The turbulent viscosity ν_t is defined by

$$\nu_t = \frac{k}{\tilde{\omega}}, \quad \tilde{\omega} = \max \left(\omega, C_{\lim} \sqrt{\frac{2 \overline{S}_{ij} \overline{S}_{ij}}{\beta^*}} \right), \tag{5}$$

with C_{lim}=7/8. The closure coefficients and auxiliary relations are

$$\alpha = 0.52, \quad \beta = \beta_0 f_\beta, \quad \beta_0 = 0.0708, \quad \beta^* = 0.09, \quad \sigma = 0.5, \quad \sigma^* = 0.6, \quad \sigma_{do} = 0.125,$$

$$\sigma_d = \begin{cases} 0 & for \quad \dfrac{\partial k}{\partial x_j} \dfrac{\partial \omega}{\partial x_j} \le 0 \\ \sigma_{do} & for \quad \dfrac{\partial k}{\partial x_j} \dfrac{\partial \omega}{\partial x_j} > 0 \end{cases} \qquad f_\beta = \frac{1 + 85 \chi_\omega}{1 + 100 \chi_\omega}, \quad \chi_\omega = \left| \frac{\overline{\Omega}_{ij} \overline{\Omega}_{jk} \overline{S}_{ki}}{\left(\beta^* \omega \right)^3} \right|,$$

where $\overline{\Omega}_{ij} = 1/2 \left(\partial \overline{u}_i / \partial x_j - \partial \overline{u}_j / \partial x_i \right)$ are the components of the rate of vorticity tensor.

Kubacki and Dick (2009) demonstrated that the latest version of the k-ω model is successful for prediction of the stagnation region of 2D plane impinging jets at low and moderate nozzle-plate distances (say for H/B<6), whereas a repair is necessary for

axisymmetric jets. The ability of the latest k-ω model, in contrast to some previous versions, to correctly predict the turbulent flow and the convective heat transfer in stagnation flow regions of plane impinging jets is mainly the result of the inclusion of the stress limiter in Eq. (5). In flow regions characterized by large levels of strain $S = \sqrt{2\bar{S}_{ij}\bar{S}_{ij}}$ (e.g. in impingement flow regions), the term $C_{\lim}\sqrt{2\bar{S}_{ij}\bar{S}_{ij}/\beta^*}$ becomes higher than ω in Eq. (5), which makes the production term P_k in Eq. (3) proportional to S instead of proportional to S^2. For boundary layer flows, the growth of the turbulent shear stress is limited in such a way that Bradshaw's assumption that the magnitude of the stress is at maximum 0.3 of the turbulent kinetic energy, is recovered. A similar stress limiter has been implemented in the SST model of Menter (1994), but in the SST model the effect of the stress limiter is restricted to the logarithmic and wake parts of the boundary layer, while in the present k-ω model the stress limiter is active everywhere (it can be active in free shear layers). As shown by Durbin (1996), a stress limiter can also be derived by imposing realizability constraints. Durbin and Petterson-Reif (2001) emphasize that generally a turbulence model will not fulfil the realizability conditions and some changes have to be made in order to ensure realizability. On the other hand, if violation of the realizability constraints is not severe in cases of interest, the changes to the underlying model can be disregarded. Wilcox (2008) emphasizes that the latest version of the k-ω model can serve as the foundation of a more general prescription of the turbulent shear stress. For example, the turbulent shear stress can be obtained with a non-linear eddy viscosity formulation or with a hybrid RANS/LES formulation. It means that condition (5) can be replaced by any other formulation if an adequate model is available. In the hybrid RANS/LES of impinging jets that we present here, the LES mode is active in the free shear layers and in the stagnation flow region. So, the limiter, meant for RANS use, has no role there. For simplicity, in the hybrid formulations, the stress limiter has been omitted everywhere, which means that Eq. (5) is redefined to (see also Davis and Dannenhoffer, 2008):

$$\nu_t^{RANS} = \frac{k}{\omega}. \tag{6}$$

With Eq. (6), the hybrid RANS/LES models reduce to a Smagorinsky-type model under the equilibrium condition, which means that the production is equal to dissipation in the k-equation (or simultaneously in the k- and ω-equations). We demonstrate later this equivalence with a Smagorinsky-type model. The consequence is that in LES mode a subgrid viscosity of Smagorinsky-type is obtained. This is wanted behaviour. The stress limiter is also omitted in the RANS mode of the hybrid formulations since it has negligible effect on the results in near-wall regions of wall parallel boundary layer flows.

3. Alternative methods of length scale substitution in the k-ω model

Three different ways of substitution of the turbulent length scale by the local grid size are described below when the hybrid RANS/LES model functions in LES mode.

In the first model, the DES-type formulation of Strelets (2001) is implemented by modifying the destruction term in Eq. (3) by

$$\beta^* k\omega = \varepsilon \rightarrow \max\left(\beta^* k\omega, \frac{k^{3/2}}{C_{DES}\Delta}\right). \tag{7}$$

The motivation for this modification is that the dissipation in the k-ω RANS model is $\varepsilon = k^{3/2}/L_t$, where the turbulent length scale is $L_t = k^{3/2}/\varepsilon = k^{1/2}/(\beta^*\omega)$. So, it means that in the dissipation term, the turbulent length scale is replaced by the grid size. The grid size is multiplied with a tuning constant C_{DES}. The constant C_{DES} has been taken from the work of Kok et al. (2004) (see also Sagaut et al., 2006), namely C_{DES}=0.67. The local grid size Δ is defined by Δ=max (Δ_x, Δ_y, Δ_z) where Δ_x, Δ_y, Δ_z denote the distances between the cell faces in x, y and z directions. A similar value of the constant C_{DES} has been determined for this model by Yan et al. (2005), namely C_{DES}=0.7. The tuning constant is always determined through simulation of the decay of isotropic turbulence. Hereafter, this model will be called the M1-model.

The second model comes from Davidson and Peng (2003) and Kok et al. (2004), (see also Sagaut et al., 2006), where the turbulent length scale has been replaced by the grid size in ν_t ,so that

$$\nu_t = \min\left(\frac{k}{\omega}, \beta^* C_{DES}\Delta\sqrt{k}\right), \tag{8}$$

and in the destruction term of the k-equation (Eq. 7). The motivation for this modification is that the RANS eddy viscosity is $\nu_t = \beta^* k^2/\varepsilon = \beta^* L_t\sqrt{k}$. So, it means that also in the eddy viscosity expression, the turbulent length scale is replaced by the grid size. The grid size is multiplied with a tuning constant C_{DES}, which again takes the value C_{DES}=0.67 by the tuning of Kok et al. (2004). This model formulation will be referred as M2-model.

The third model is based on inclusion of the local grid size only in the definition for ν_t. As shown by Magnient et al. (2001) and De Langhe et al. (2005) (see also Sagaut et. al., 2006), an LES subgrid viscosity can be expressed by

$$\nu_t = C_e \Delta^{4/3} \varepsilon^{1/3}, \tag{9}$$

where Δ is the cut-off length, $C_e = \left(\frac{3C_K}{2}\right)^{-1} \pi^{-4/3}$, with C_K the Kolmogorov constant (C_K is 1.4 to 1.5). So, C_e is about 0.10.

A RANS-type eddy viscosity can be written as

$$\nu_t^{RANS} = \beta^* \frac{k^2}{\varepsilon} = \beta^* L_t^{4/3} \varepsilon^{1/3}. \tag{10}$$

Equations (9) and (10) have the same structure. So, if C_e is approximated by β^*=0.09 for the sake of the hybridization (Sagaut et al, 2006), the LES subgrid viscosity can be written as

$$\nu_t = \beta^* \Delta^{4/3} \varepsilon^{1/3} \qquad \text{or} \qquad \nu_t = \nu_t^{RANS} (\Delta / L_t)^{4/3} \tag{11}$$

The term $(\Delta/L_t)^{4/3}$ in Eq. (11) can be seen as a latency factor $f(\Delta,L_t)$ in the sense of Batten et al. (2004), which reduces the RANS eddy viscosity to an LES subgrid viscosity. As in the other models, we introduce a tuning constant C_{DES} which multiplies Δ. The function $(C_{DES}\Delta/L_t)^{4/3}$ is limited by unity in order to recover the RANS turbulent viscosity for $L_t < C_{DES}\Delta$. This results in

$$f\left(\Delta, L_t\right) = \min\left[\left(\frac{C_{DES}\Delta}{L_t}\right)^{4/3}, 1\right]. \tag{12}$$

If the turbulent length scale L_t is smaller than the local grid size $C_{DES}\Delta$ in Eq. (12) (e.g. close to walls), the model acts in RANS mode. Otherwise, if the turbulent length scale L_t is higher than the local grid size $C_{DES}\Delta$, the RANS turbulent viscosity is reduced by the function $f(\Delta,L_t)$ and becomes a subgrid viscosity. We refer to this model as the M3-model. For reasons of consistency with model M2, as we discuss hereafter, the value of C_{DES} is set to 0.67.

Table 1 summarizes the definitions of the D_k and ν_t in a unified way for the models M1, M2 and M3.

The hybrid models considered here reduce to a Smagorinsky subgrid model in LES mode under equilibrium conditions. Table 2 summarizes the equilibrium conditions and the corresponding values of the Smagorinsky constant C_s. Two Smagorinsky coefficients can be derived for the M1-model under the local equilibrium conditions (production is equal to destruction simultaneously in both k- and ω-equations). This is due to the dependence of the β-coefficient on the flow dependent parameter f_β in the ω-equation. Our experience is that for plane impinging jets, the lower value of the Smagorinsky constant, C_s=0.13 (corresponding to β= 0.06) is obtained in LES mode. The higher value of the Smagorinsky constant, C_s=0.15 (corresponding to β= 0.0708) is only obtained close to walls, so it is not relevant for the LES zone. The models M2 and M3 have the same value of the Smagorinsky constant (C_s=0.11) under the assumption of local equilibrium. It permits to use the same value of C_{DES} for the M2 and M3 hybrid models. For these models, we took the value of C_{DES} as determined by Kok et al.(2004), based on simulation of decaying isotropic turbulence with a high-order numerical scheme for discretization of the convective terms in the flow equations. Here we use a low-order numerical scheme for spatial discretization. We take this into account in the analysis of the results discussed later. The same value of the C_{DES} constant has been used for the model M1. As mentioned, it gives a somewhat higher value of the Smagorinsky constant (C_s=0.13) than for the other models (C_s=0.11). However, our numerical results show that the level of modelled turbulent kinetic energy by the model M1 is comparable to that of the M2-model. We will illustrate this further.

4. Computational aspects

Three cases are considered in the present work. For the hybrid RANS/LES model simulations, the computational domain consists of a rectangular box. Details related to the size of the computational domain are summarized in Table 3. The size of the computational domain W in the spanwise direction is set to πB. Similarly, in the LES computations of Tsubokura et al. (2003), $W=\pi B$ while in the LES of Cziesla et al. (2001) $W=2B$. We note that in the LES computations of Beaubert and Viazzo (2002, 2003) $W=2\pi B$, but this is at the cost of reducing the grid resolution in the spanwise direction. Figure 1 shows a scheme of the computational domain. The 2D RANS computations were done on 2D domains which are x-y planes of the 3D domains.

At the inlet to the computational domain (nozzle exit) an almost flat mean velocity profile was specified according to Tsubokura et al. (2003):

$$V(x,0,z) = -V_0\left(1-(2x/B)^{14}\right), \tag{13}$$

where V_0 denotes the mean velocity in the symmetry plane.

As shown in Figure 2, the profile defined by Eq. (13) agrees well with the experimental data of Maurel and Solliec (2001). The same definition of the inlet mean velocity profile was used for all cases.

As noted by Maurel and Solliec (2001), a uniform profile of the fluctuating velocity component can be assumed at the jet exit. In the experiments, the nozzle exit turbulence intensity varied in the range Tu=1.6-2.8% for the nozzle-plate distance H/B=10 and Re=13500. For the other cases (H/B=9.2 and 4, and Re=20000), the turbulence intensity was equal to Tu=1% (Ashforth-Frost et al., 1997, Zhe and Modi, 2001). The turbulence length scale was not measured. In the present RANS computations, constant profiles of k and ω were specified at the inlet of the computational domain with Tu=2.5% for H/B=10 and Re=13500 and Tu=1.0% for H/B=9.2, 4 and Re=20000 while $l_{t,inl}=0.16(\beta^*)B=0.015B$, according to Jaramillo et al. (2008). The inlet values of the turbulent quantities were set to $k_{inl}=1.5(Tu\ V_0)^2$ and $\omega_{inl}=(k_{inl})^{0.5}/l_{t,inl}$. For the hybrid model simulations, the vortex method of Fluent was used to generate the resolved fluctuations at the jet exit (Mathey et al., 2006). In order to keep the sum of resolved and modelled turbulence intensity at the jet exit equal to that reported in the measurements, the inlet profiles of k and ω were adjusted in the core of the flow. We assigned small values of k and ω to the modelled fluctuations while the remaining part was assigned to the resolved perturbations. The inlet turbulence intensity, Tu, was split into two parts, with 10% of the total (measured) turbulence intensity corresponding to the modelled energy and 90% to the resolved energy. The length scale $l_{t,inl}$ was set to the same value in the modelled and resolved parts. Tests showed that the precise way in which the inlet energy is split into modelled and resolved energy is not very crucial for simulation of the plane impinging jet. The reason is that the shear layers at the jet exit are in RANS mode. So, the flow dynamics in the shear layers of the jet depends strongly on the way in which the hybrid RANS/LES model recovers the LES mode downstream of the jet exit. At the outflow boundaries, pressure outlet boundary conditions were applied with a zero normal

gradient for the modelled scalars. At the walls, no-slip conditions were used with the turbulent quantities computed according to Menter (1994):

$$k = 0, \quad \omega = 10\frac{6\nu}{\beta_0 (\Delta y)^2}, \tag{14}$$

where Δy is the first point away from the wall. Periodic boundary conditions have been applied in the spanwise *z* direction.

In the present hybrid RANS/LES computations, the computational grid consists of a total number of $N \approx 1.1$ million grid points for the first case (*H/B*=10, *Re*=13500), $N \approx 1.6$ million grid points for the second case (*H/B*=9.2, *Re*=20000) and $N \approx 0.9$ million grid points for the third case (*H/B*=4, *Re*=20000). In the reference LES computations of Beaubert and Viazzo (2002, 2003) (*H/B*=10 and *Re*=13500), the computational mesh had 240 x 150 x 64 cells ($N \approx 2.3$ million). The number of grid points has been mainly reduced in the x-direction, compared to the LES simulations of Beaubert and Viazzo (2002, 2003). The grid points have been clustered towards the walls (in order to fulfil the condition $y^+ < 3$) and in the shear layer of the jet, since these are the regions of high velocity gradients. Uniform grid spacing was used in the spanwise z direction. Figure 3 shows the computational mesh in the xy-plane at distance |x/B|<6 and a close-up of the computational mesh in vicinity of the jet exit for H/B=10 and Re=13500. The grid is fine enough in the vicinity of the jet exit so that mixing layers enter very fast into LES mode, as we demonstrate further. For two cases, *H/B*=10, *Re*=13500 and *H/B*=9.2, *Re*=20000, we also used fine grids of about 3.8 and 5.4 million grid points, respectively. Details on the grids are summarized in Table 3.

The 2D RANS computations were done on grids with 270x390 cells for a basic grid and 570x780 cells for a fine grid. We demonstrate later for the case H/D=10, Re=13500 that the basic computational grid for the 2D RANS simulations is fine enough, so that grid independent solutions are obtained.

The computations have been performed with the Fluent code ver. 12, for constant density fluid. The transport equations were implemented with UDFs. The bounded central differencing scheme was applied for the convective terms in the momentum equations and the second order upwind scheme for the convective terms in the energy, k- and ω-equations. For temporal discretization, a second-order implicit scheme was applied. At each time step, the residuals for momentum and transport equations fall below 1e-5. Typically, about 15 to 20 inner iteration steps were required to obtain a converged solution at each time step.

The heat transfer is modelled with the energy equation

$$\frac{DT}{Dt} = \frac{\partial}{\partial x_j}\left(\left(\frac{\nu}{\mathrm{Pr}} + \frac{\nu_t}{\mathrm{Pr}_t}\right)\frac{\partial T}{\partial x_j}\right), \tag{15}$$

where T is the mean temperature, Pr and $\mathrm{Pr_t}$ are the laminar and turbulent Prandtl numbers, respectively Pr=0.74, $\mathrm{Pr_t}$=0.85. The Nusselt number is defined by

$$\mathrm{Nu} = \frac{-(\partial \mathrm{T}/\partial \mathrm{y})_\mathrm{w} \mathrm{B}}{(\mathrm{T_w} - \mathrm{T_i})}, \tag{16}$$

A constant value of the temperature T_w =310K was imposed on the impingement plate. The inlet temperature was set to T_i =300K. The remaining walls are adiabatic.

5. Results

Results of the simulation of plane jets impinging onto a flat plate are presented for the k-ω RANS and the hybrid RANS/LES models. The results are compared to the experimental data of Maurel and Solliec (2001), Asforth-Frost et al. (1997), Zhe and Modi (2001), Tu and Wood (1996) and to the LES results of Beaubert and Viazzo (2002, 2003).

5.1. Instantaneous flow field

Fig. 4 (a) shows an instantaneous field of the velocity magnitude and (b) an instantaneous field of $f = \min(1, C_{DES}\Delta/L_t)$ in the x-y plane for H/B=10 and Re=13500, obtained with the M2-model. The instantaneous velocity field shows the dynamics of the impinging jet in the LES zone, which corresponds to the values of $f < 1$. As shown in Fig. 4 (b), the RANS zone ($f = 1$) is active close to walls due the grid size $C_{DES}\Delta$ being larger than the turbulent length scale L_t. The RANS zone is also active in the middle of the channel at larger distances from the symmetry plane $|x/B| > 15$ (not shown), where the dynamics of the large scale structures becomes negligible and the grid becomes too coarse to resolve the flow unsteadiness. The plots of the instantaneous velocity magnitude are very similar for all three models (not shown for M1 and M3). The plots of the f-values are similar for the models M1 and M2 (not shown for M1). The f-value of the M3-model (not shown) is lower than for the models M1 and M2. But the role of the f-value for the M3-model is quite different from the role of this factor in the models M1 and M2. For the M3-model, it is the reduction factor of a more RANS-like viscosity.

Contour plots of modelled k are shown in Fig. 5 for all model formulations in the x-y plane located at $z/B=\pi/2$ for H/B=9.2 and Re=20000. We recall that the M1-model consists of the substitution of the turbulent length scale by the local grid size in the destruction term of the k-equation, the M2-model uses the substitution in the k-equation and in the definition for ν_t, while the M3-model introduces the grid size only in the definition for ν_t. The instantaneous fields of subgrid k obtained with the models M1 and M2 are quite similar. The instantaneous field of k obtained with the M3-model strongly differs from those obtained with the models M1 and M2. Much higher levels of modelled turbulent kinetic energy are obtained with the M3 model, but only a fraction of this turbulent kinetic energy is used in the definition of the eddy viscosity through the latency factor. We note that it is difficult to say what exactly this fraction is.

Figure 6 shows the counter-rotating longitudinal vortices in the stagnation flow region, at distance x/B=-0.5 from the symmetry plane, for H/B=10, Re=13500 (normalized velocity vectors are shown in the z-y plane). The cut at z/B=1.5 shows the strength of the vortices in the x-direction. These counter-rotating vortices, also known as Görtler vortices, were observed in the stagnation flow region of a plane impinging jet by Sakakibara et al. (1997) and Maurel and Solliec (2001). They have been also reproduced in the simulations of Beaubert and Viazzo (2002, 2003) using LES and in the simulations of Tsubokura et al. (2003) using LES and DNS. As mentioned by Tu and Wood (1996), these vortices appear as an effect of angular momentum instability in flow regions

characterized by convex streamline curvature. According to Tu and Wood (1996), the Görtler vortices lower the wall shear stress. This means that the shear stress is lower than obtained from the analytical solution of the laminar Hiemenz flow. Correct prediction of the lowering of the wall shear stress by these counter-rotating vortices might therefore have some importance, since their effect counteracts the increase of the wall friction by turbulence coming from the shear layer of the jet.

5.2. Jet expansion and jet impact

Figure 7 shows the mean and fluctuating y-velocity evolution in the symmetry plane and the skin friction coefficient along the impingement plate for RANS simulations of the plane impinging jet at H/B=10 and Re=13500 on the basic and fine grids. The results on the basic grid (270x390) are almost identical to the results on the fine grid (570x780). So essentially, grid independent results have been obtained. Further, the results on the basic grid will be used for comparison with the results from the hybrid RANS/LES models.

Figures 8 and 9 show the mean and fluctuating y-velocity evolution in the symmetry plane, obtained with the different hybrid RANS/LES formulations and the experimental data of Maurel and Solliec (2001), the LES results of Beaubert and Viazzo (2002) and 2D RANS results obtained with the k-ω model. For the hybrid methods, the data have been averaged in time and in the spanwise z direction.

The results obtained with the pure RANS model are erroneous. With RANS, the length of the jet core is strongly overpredicted with respect to the measured value and the value computed by LES and hybrid RANS/LES. The fluctuating velocity component predicted by RANS, computed as $\sqrt{2k/3}$, slightly decays with increasing distance from the nozzle exit while in reality the fluctuation rises already at y/B=2. The poor performance of the RANS model is due to too weak production of turbulent kinetic energy in the shear layer of the jet. For the test case that we discuss here, physically, the expanding shear layers at the edges of the plane jet merge before the impact of the jet on the plate, but in the RANS-simulation the merging is not yet reached. A similar conclusion was drawn by Fernandez et al. (2007), where application of various RANS models (also the k-ω model) for simulation of twin plane impinging jets showed underprediction of the turbulence mixing in the shear layers of the jets. Georgiadis et al. (2006) included some modifications into the eddy-viscosity RANS models in order to repair for this underestimation of the turbulent mixing in the jet core region. We notice that the poor performance of the RANS model for impinging jet simulation at large nozzle-plate distance is in contrast with its good performance for small distance between jet exit and impingement plate, as demonstrated by Kubacki and Dick (2009).

The results obtained with the hybrid RANS/LES methods are close to each other and show good agreement with the experimental data and the LES. The observation that all hybrid results give similar results is not particularly surprising. Methods M2 and M3 have the same theoretical limit value of the Smagorinsky constant, while method M1 has a slightly higher value. So, already based on this analytical property, we can know that the methods are approximately equivalent. In Figure 9, in particular, the rise of the fluctuating velocity around y/B=2 is very well predicted. This means that the grid is fine enough to allow activation of the LES mode where the mixing of the shear layers becomes significant. The mean velocity profiles reveal that the jet mixes somewhat too fast in the hybrid simulations with respect to the experimental data and the LES results.

The resolved fluctuating velocity profiles are close to the resolved fluctuating velocity profile of the LES and close to the experimental fluctuating velocity profile. There is no information on the modelled fluctuating velocity components and the modelled shear stress in the reference LES of Beaubert and Viazzo (2002, 2003). So, for the reference LES, we can only show the resolved parts. From the comparison in figure 9 with the experimental values of the fluctuating velocity components, we can assume that the hybrid RANS/LES results of the total fluctuating velocity components are also somewhat above those of the LES. The too high value by the hybrid RANS/LES means that the turbulence production in the hybrid models is somewhat too large. For the same grid resolution (1.1 million grid points), the M3-model predicts the highest values of the fluctuating velocity and the M1-model predicts the lowest values. We also performed a simulation of the plane impinging jet on a finer grid with about 3.8 million grid points with the M2-model. The mean velocity profile (dashed line with symbols in figure 8b) is now very close to the experimental profile and the profile from the LES. The profile of the resolved fluctuating velocity (dashed line with symbols in figure 9b) is still somewhat above the profile from the LES and the profile of the total fluctuating velocity (dashed line with symbols in figure 9d) is still above the experimental profile, but the results come much closer than for the basic grid. This observation shows that on the fine grid there is still somewhat too much turbulence production in the hybrid simulation. The explanation is that the vortex structures in the shear layers of the jet are reproduced somewhat too big in the LES mode of the hybrid models, as a consequence of the somewhat too dissipative character of the numerical technique (TVD-discretization in the momentum equations) so that the break-up of the structures is somewhat delayed. In the reference LES, fourth order compact differences are used in the non-homogeneous directions and a Fourier pseudo-spectral method in the spanwise homogeneous direction. In general, structures that are too big generate too high resolved stresses (Piomelli et al., 2008).

Although the results obtained on the basic grid with about 1.1 million grid points are somewhat too diffusive, which obscures a bit the comparison, we can conclude that the three hybrid approaches that we study here are largely equivalent for the prediction of the mixing of the plane jet approaching the impingement plane. We will compare other aspects further. We will also use fine grid results for model M2.

Figures 10 and 11 show the resolved and total Reynolds stress along x-lines located at different distances from the jet exit. Similarly to the velocity profiles, the Reynolds stress $\langle u'v' \rangle/(V_0)^2$ was averaged in time and in spanwise z direction. The results are compared to the experimental data of Maurel and Solliec (2001) and to the LES results of Beaubert and Viazzo (2002). At distance y/H=1/12 from the jet exit (Fig. 10) the shear layers begin to develop. The Reynolds stress predicted by RANS has a peak value of $\langle u'v' \rangle/(V_0)^2$=0.005 at x/B=0.5, which is in very good agreement with the experimental value (Fig 10, c). This correspondence shows that the inlet conditions are set correctly. At y/H=1/12, the resolved Reynolds stress produced by the hybrid RANS/LES models is smaller than the measured Reynolds stress (Fig. 10, a) and the shear stress predicted by the M2-model (basic and fine grids) is much smaller than the shear stress by LES (Fig 10, b). The peak value of the total Reynolds stress by the hybrid models is, like for RANS, very close to the experimental value (Fig. 10, c and d). The peak value produced by the LES seems to be too high. The differences between the different hybrid RANS/LES

implementations are marginal at *y/H*=1/12. Again, the good correspondence with experiments shows that the inlet conditions are set correctly for the hybrid RANS/LES. We note that at position y/H=1/12 still a large part of the Reynolds stress is modelled in the hybrid simulations (about 50%). This is the consequence of the relative coarse grid, since the shear layer is captured by only 6 cells.

At distance *y/H*=0.5 (Fig. 11), the Reynolds stress is much underpredicted by RANS close to the symmetry plane. This result confirms the strong underprediction of the mixing by RANS. Some differences in the resolved Reynolds stress between the various hybrid RANS/LES approaches are visible at distance *y/H*=0.5. All hybrid models slightly overpredict the maximum of $\langle u'v' \rangle/(V_0)^2$. We remark that the modelled part in the Reynolds stress is negligible in the hybrid simulations at distance *y/H*=0.5. This means that the grid is now fine enough to almost fully resolve the structures in the mixing layer. We verified that for the basic grid simulations, the maximum ratio of the modelled to the total normal stress $\langle v'v' \rangle/(V_0)^2$ (axial component) along the symmetry plane and along the x-line at *Y/H*=0.5 is about 8%, while the maximum ratio of the modelled to the total shear stress $\langle u'v' \rangle/(V_0)^2$ is approximately 3% (Fig. 11, a and c). A high level of total shear stress returned by the hybrid RANS/LES model on the basic grid (Fig. 11), with more than 97% contribution of the resolved part, might be an indication that the eddy-viscosity based hybrid RANS/LES models generate somewhat too much turbulent viscosity in the vortex core regions which delays the vortex break-up process. We also remark that overprediction of the Reynolds stress remains, but becomes much less, for the M2-model at the fine grid (3.8 million grid points). Again, it is difficult to formulate quantitatively the ability of the hybrid RANS/LES models to converge towards LES on grid refinement, due to lack of information about the subgrid-scale component in the LES computations of Beaubert and Viazzo (2003). But, the convergence is obvious in figures 11, b and d.

Figure 12 shows the profiles of the skin friction (scaled with $Re_b=b_pV_0/\nu$, where b_p is the half-width of the impingement pressure profile) along the impingement plate in the impact zone. The hybrid RANS/LES results are again compared to experimental data (Tu and Wood, 1996), to LES results (Beaubert and Viazzo, 2002, 2003) and to the 2D RANS results. We note the differences in the nozzle-plate distances and Reynolds number between the experimental data of Tu and Wood (1996) and the present results. In Tu and Wood (1996), the nozzle-plate distances were *H/B*=8 and 12 (in contrast to *H/B*=10 in the present simulations) and the Reynolds number was *Re*=11000 (in the present simulations *Re*=13500). The peak values of the skin friction predicted by RANS are higher than the peak values obtained with the hybrid RANS/LES (Fig. 12 a). As discussed above, this is due to the overprediction of the length of the core (or underestimation of the jet expansion) using the k-ω model. For this case, the RANS solution agrees very well with LES at larger distances from the symmetry plane (for $x/b_p>2$). All hybrid models predict peak values around $|x/b_p| = 1$ in good agreement with the experimental data (Fig. 12, a). The results obtained with the M2 model on the basic and fine grids are close to each other and are in good agreement with the LES results of Beaubert and Viazzo (2002) (Fig. 12, b). The agreement between computed values using the hybrid RANS/LES methods, pure RANS and LES is good at larger distances from the symmetry plane (at $|x/b_p|>2$).

Overall, the predictions by the hybrid models (Figures 8 to 12) are quite good for the expanding jet and the impact zone. As explained before, this is the consequence of the LES representation of the shear layers of the jet. The hybrid models generate somewhat too high Reynolds stresses in the expanding jet. The best agreement between computations and measurements is obtained with the M1-model, but the differences between the models are small.

5.3. Developing wall jet and developed wall jet

Figure 13 shows profiles of computed mean x-velocity components and the comparison with the experimental data of Asforth-Frost et al. (1997) and Zhe and Modi (2001) along a line perpendicular to the impingement plate at different distances from the symmetry plane for simulation of the plane impinging jet at H/B=9.2 and Re=20000. First of all, quite large differences are visible between the experimental data of Asforth-Frost et al. (1997) and Zhe and Modi (2001) at distances x/B=1 and x/B=5 (Fig. 13, a and c). At distance x/B=1 the mean velocity profile obtained with the pure k-ω model is strongly overpredicted. We do not have experimental data on the velocity profiles in the impacting jet, but we can assume, based on the observations discussed before, that there is too weak turbulence mixing in the shear layer of the jet in the RANS simulation. This gives then an explanation for the too high momentum in the developing wall jet. With the hybrid RANS/LES models much better correspondence is obtained with the experimental data. There is an underprediction of the velocity level. We do not have experimental data on the Reynolds stresses in the impacting jet, but we can assume, based on the observations discussed before, some overprediction of the Reynolds stress in the impacting jet, causing somewhat too low momentum in the developing wall jet. At distance x/B=2 (Fig. 13, b) the mean velocity profile predicted with the k-ω model still deviates strongly from the experimental profile. The hybrid models still underpredict the velocity level. At x/B=5 (Fig. 13, c), all simulation results come closer to the experiments. This shows that the asymptotic behaviour of all models is basically correct.

Figure 13 shows also the results obtained with the M2-model on a refined grid (5.4M). Here, in contrast to the previously discussed results for the expanding jet (test case H/B=10, Re=13500, Fig. 8-12), the difference between the fine grid (5.4M) and the basic grid (1.6M) results is small. It demonstrates that the results obtained with the hybrid M2-model are to a large extent grid independent in the RANS-dominated flow region (in the developing wall jet). The results show that on the fine grid there is still somewhat too much turbulence production by the M2-model in the wall jet region. We observe a relatively large underprediction of the data with the M2-model on the refined grid at X/B=2 (Fig.13, b), but this happens in the region where the simulation transitions from LES to RANS and so, is the most delicate. We note, however, that due to the large difference between the two sets of experimental data, it is difficult to judge precisely on the quality of the hybrid results in the developing wall jet and the developed wall jet regions.

Figure 14 shows the skin friction coefficient along the impingement plate obtained with the RANS k-ω model and computed with the hybrid RANS/LES formulations. RANS predicts the skin friction coefficient far too high in the impingement region and also in the developing wall jet region. As mentioned above, this is caused by underprediction of

the turbulence mixing in the shear layer of the jet which results in too slow spreading of the mean velocity profiles into the free stream as the flow turns into a wall jet. With the hybrid RANS/LES methods, much better correspondence between computations and experiment is obtained. The peak value of c_f at x/B=2 is slightly overpredicted with all hybrid RANS/LES formulations and even at larger distance from the impingement zone, overprediction remains. We should, however, note that the experimental values of the skin friction coefficient are probably somewhat too low. The skin friction has been determined with hot-wire anemometry and this technique is not fully accurate very close to walls.

Figure 15 shows the distribution of the Nusselt number along the impingement plate and its comparison with the experimental data of Ashforth-Frost et al. (1997). RANS is not able to correctly reproduce the monotonic decay of the Nusselt number profile with increasing distance from the symmetry plane (even if the stagnation point Nusselt number is well predicted). There is, again, little difference between the three hybrid models.

5.4. Small nozzle-plate distance

Finally, the results of plane impinging jet simulation at low nozzle-plate distance H/B=4 and Re=20000 are discussed with application of the RANS and M2 hybrid RANS/LES models. For small nozzle-plate distance, the core of the jet flow impinges on the plate. This means that, in contrast to the cases discussed before, the mixing of the two jet edges is not completed at impingement.

As mentioned above, the pure RANS k-ω model is quite successful for prediction of 2D plane impinging jets at low and moderate nozzle-plate distances. This is a beneficial effect of the stress limiter. Here we demonstrate quite good performance of the RANS model for simulation of plane impinging jet at H/B=4 and Re=20000. Fig. 16 shows profiles of the x-velocity component along lines perpendicular to the impingement plate at distances x/B=1, 2, 5 and 7 obtained with RANS and the hybrid M2-model. The simulation results are compared with experimental data of Asforth-Frost et al. (1997) and Zhe and Modi (2001). Here, the experimental data of Asforth-Frost et al. (1997) and Zhe and Modi (2001) are somewhat less different in the near-wall region (for $(H-y)/B$<0.1) at distances x/B>1 than for the high nozzle-plate distance case (Fig. 13). So, a more trustworthy comparison of the computed and measured mean velocity profiles can be done. The k-ω RANS model is able to correctly reproduce the flow acceleration at distances x/B=1 and 2 (Figure 16, a and b) and predicts somewhat too slow flow deceleration further downstream (Figure 16, c and d). Based on the analysis of the previous cases, we can conclude that this is due to too weak production of turbulent kinetic energy in the shear layer of the jet. The mean velocity profiles are very well reproduced by the hybrid RANS/LES method at all distances from the symmetry plane, except for x/B =5 where the correspondence with the experiments is less good.

Figure 17 shows the evolution of the skin friction coefficient along the impingement plate obtained with the k-ω RANS and the hybrid M2-model and their comparison with the experimental data of Zhe and Modi (2001) for H/B=4 and Re=20000. The maximum of c_f at $x/B \cong 1$ is overpredicted with respect to the experimental results by both the k-ω RANS and the hybrid model. For larger values of x/B, the result by the hybrid model is

close to the experimental data, while there is overprediction by the RANS model. That for small distance x/B (x/B<2) the RANS and hybrid results coincide is in accordance with the almost identical velocity profiles shown on Figure 16, a and b. In the impingement zone, the flow is quasi-laminar, which means that there is a very low turbulence level. The low turbulence level is reproduced by the RANS model thanks to the stress limiter. In the hybrid simulation, the core of the jet flow in the impingement zone is in LES mode with almost zero turbulence activity. So, essentially, the skin friction coefficient for small values of x/B is a laminar value for both models, and since the velocity profiles are correct near to the wall (Fig. 16), principally, cannot be in error. So, again, we have to doubt somewhat the experimental values of the skin friction coefficient. For larger x/B the overprediction of the skin friction by the RANS model is due to the too low mixing in the shear layer.

Figure 18 shows the evolution of the Nusselt number. The stagnation point Nusselt number predicted by the k-ω RANS and the hybrid model are in excellent agreement with the experimental data of Asforth-Frost et al. (1997). The explanation is that the impingement zone is quasi-laminar and that this is captured by both the RANS model and the hybrid model. The further evolution of the Nusselt number profile is better predicted by the hybrid RANS/LES model than by the k-ω RANS model. In particular, the dip in the profile is captured by the hybrid model.

The conclusion, for simulation of a plane impinging jet at low nozzle-plate distance, is that the improvements obtained with the hybrid RANS/LES model over the RANS model are much smaller than for larger nozzle-plate distance. The good prediction by RANS for small nozzle-plate distances is due to the role of the stress limiter. In RANS, the stress-limiter has no beneficial effect at large nozzle-plate distance between the nozzle jet exit and the impingement plate owing to strong underestimation of the turbulence mixing in the shear layer of the jet.

6. Summary

The performance of hybrid RANS/LES models based on the latest version of the k-ω model of Wilcox (2008) for simulation of plane jets impinging onto a flat plate has been analysed. Three different ways of substitution of the turbulent length scale by the local grid size in LES mode have been tested. With the M1-model, the local grid size is introduced in the destruction term of the k-equation, while for the M2-model the local grid size is introduced in both the destruction term of the k-equation and in the definition of ν_t . The M3-model is based on damping of the RANS turbulent viscosity by a latency factor. In LES mode, the three models lead to a Smagorinsky subgrid scale model under equilibrium conditions. The Smagorinsky constants of models M2 and M3 are exactly the same, while the constant of model M1 is somewhat higher. So, basically, one can expect similar behaviour of the models in LES mode. Plane impinging jets with nozzle-plate distances H/B=10, 9.2 and 4 and Re=13500, 20000 were simulated. The predicted skin friction on the plate, heat transfer to the plate, Reynolds stresses profiles and velocity profiles were compared with experimental data and results from reference LES. Generally, the three hybrid models perform quite well and there are only minor differences between their results. Compared to the basic RANS k-ω model, the hybrid RANS/LES models are much better for simulation of plane impinging jets at high nozzle-

plate distances. This is due to the strong underestimation by RANS of the turbulent mixing in the shear layer of the jet. For small nozzle-plate distance, the error in the turbulent mixing by the RANS model has less severe consequences, but still the results by the hybrid RANS/LES model are better.

Appendix. Eddy viscosity models in large eddy simulation.

In this appendix, we give an overview of the relationships relevant for eddy viscosity modelling in large eddy simulation. This information helps to understand the modelling approaches discussed in section 3. The overview is based on the work of Giles (1994a, 1994b), Lesieur (1997), Magnient et al. (2001) and De Langhe et al. (2005a, 2005b). The values of the constants and the relationships between the constants may differ somewhat in other literature sources, but these small differences are finally not relevant for modelling, as common approximations lead to the same final results.

A1. The Kolmogorov energy spectrum

The distribution of the turbulent kinetic energy over the wave number spectrum in the inertial subrange is

$$E(\Lambda) = C_K \varepsilon^{2/3} \Lambda^{-5/3}, \qquad \text{(A1)}$$

with Λ the wave number, $\Lambda = \pi/\Delta$, where Δ is the half wave length. C_K is the Kolmogorov constant with value around 1.4 to 1.5.

A2. Relationship between ε, Λ_c and k_c

For $\Lambda_c = \pi/\Delta$, a cut-off wave number in the inertial range, and k_c the turbulent kinetic energy of the scales smaller than Δ, for homogeneous turbulence, the relationship is

$$\varepsilon = \frac{\Lambda_c}{(\frac{3C_K}{2})^{3/2}} k_c^{3/2} = \pi(\frac{3C_K}{2})^{-3/2} \frac{k_c^{3/2}}{\Delta} = C_o \frac{k_c^{3/2}}{\Delta}, \qquad \text{(A2)}$$

with
$$C_o = \pi(\frac{3C_K}{2})^{-3/2} = 0.93 \text{ to } 1.03 \qquad \text{(A3)}$$

The constant C_o is almost universally approximated by unity and the relationship (A2) with C_o=1 is assumed to be generally valid.
The simplification implies

$$C_K = \tfrac{2}{3} \pi^{2/3} = 1.43. \qquad \text{(A4)}$$

A3. Eddy viscosity in function of ε and Λ_c

For homogeneous isotropic turbulence generated by forcing the Navier-Stokes equations, one obtains

$$\nu_{LES} = a\,\varepsilon^{1/3}\Lambda_c^{-4/3} = C_e\,\varepsilon^{1/3}\Delta^{4/3} \qquad \text{(A5)}$$

where $$a = (\frac{3C_K}{2})^{-1} = 0.44 \text{ to } 0.48$$

and $$C_e = (\frac{3C_K}{2})^{-1}\pi^{-4/3} = 0.097 \text{ to } 0.103 \qquad \text{(A6)}$$

A4. Eddy viscosity in function of Δ and k_c

Through substitution of ε from (A2) into (A5) one obtains

$$\nu_{LES} = C_q\ k_c^{1/2}\Delta \qquad \text{(A7)}$$

where $$C_q = C_e C_o^{1/3} = (\frac{3C_K}{2})^{-3/2}\pi^{-1} = 0.094 \text{ to } 0.105 \qquad \text{(A8)}$$

A4. Eddy viscosity in function of ε and k_c

Through substitution of Δ from (A2) into (A5) one obtains

$$\nu_{LES} = C_\mu\, k_c^2/\varepsilon\,, \qquad \text{(A9)}$$

where $$C_\mu = C_e C_o^{4/3} = (\frac{3C_K}{2})^{-3} = 0.088 \text{ to } 0.108 \qquad \text{(A10)}$$

A6. Unique values of C_e, C_q and C_μ

The values of C_e, C_q and C_μ become identical for $C_o = 1$. This is reached for the value of the Kolmogorov constant $C_K = \frac{2}{3}\pi^{2/3}$ (A4). Then $C_e = C_q = C_\mu = \pi^{-2} = 0.101$. Mostly $C_e = C_q = C_\mu$ are identified with the constants of the eddy viscosity expressions $C_\mu = \beta^*$ from a k-ε or a k-ω model, so that

$$C_e = C_q = C_\mu = 0.09 \qquad \text{(A11)}$$

This gives better correspondence with experiments. Even lower values of $C_e = C_q = C_\mu$ are sometimes used in large eddy simulations.

A7. Smagorinsky eddy viscosity

The expression is

$$\nu_{LES} = \ell_0^2 \left|\overline{S}\right| = (C_s \Delta)^2 \left|\overline{S}\right| \quad \text{with} \quad \left|\overline{S}\right| = \sqrt{2\overline{S} : \overline{S}} \tag{A12}$$

For homogeneous turbulence, one obtains

$$(\overline{S})^2 = \pi^{4/3} (\frac{3}{2} C_K) \varepsilon^{2/3} \Delta^{-4/3} \qquad \text{or} \qquad \varepsilon = (\frac{3}{2} C_K)^{-3/2} \pi^{-2} \Delta^2 (\left|\overline{S}\right|)^3 \tag{A13}$$

For equilibrium: $\nu_{LES} (\overline{S})^2 = \varepsilon$. This gives for the Smagorinsky constant

$$C_s = \frac{\ell_o}{\Delta} = (\frac{3}{2} C_K)^{-3/4} \pi^{-1} = 0.173 \text{ to } 0.183 \tag{A14}$$

We remark that $C_s = C_e^{3/4}$ (A15)

The Smagorinsky constant is usually lowered to around 0.10, in order to obtain better correspondence with experiments in shear flow applications.

Acknowledgement

The authors acknowledge the support from the research project 'Novel Multiscale Approach to Transport Phenomena in Electrochemical Processes' (IWT, contract: MuTEch SBO 040092)

References

Ashforth-Frost, S., Jambunathan, K., Whitney, C.F., 1997. Velocity and turbulence characteristics of a semiconfined orthogonally impinging slot jet, Experimental Thermal and Fluid Science 14, 60-67.

Batten, P., Goldberg, U., Chakravarthy, S., 2004. Interfacing statistical turbulence closures with large-eddy simulation, AIAA Journal 42, 485-492.

Beaubert, F., Viazzo, S., 2002. Large eddy simulation of a plane impinging jet, C.R. Mecanique 330, 803-810.

Beaubert, F., Viazzo, S., 2003. Large eddy simulations of plane turbulent impinging jets at moderate Reynolds numbers, Int. J. Heat Fluid Flow 24, 512-519.

Cziesla, T., Biswas, G., Chattopadhyay, H., Mitra, N.K., 2001, Large-eddy simulation of flow and heat transfer in an impinging slot jet, Int. J. Heat Mass Transfer 22, 500-508.

Davis, R.L., Dannenhoffer, J.F., 2008. Detached-eddy simulation procedure targeted for design, J. of Propulsion Power 24, 1287-1294.
Davidson, L., Peng, S.H., 2003. Hybrid LES-RANS modelling: a one-equation SGS model combined with a k-ω model for predicting recirculating flows, Int. J. Numer. Meth. Fluids 43, 1003-1018.

De Langhe, C, Merci, B., Dick, E., 2005a. Hybrid RANS/LES modelling with an approximate renormalization group. I: model development. J. Turbulence 6 (13), 1-18.

De Langhe, C, Merci, B, Lodefier, K, Dick, E.,2005b. Hybrid RANS/LES modelling with an approximate renormalisation group II: Applications. J. Turbulence 6 (14), 1-16.

Durbin, P.A., 1996. On the k-ε stagnation point anomaly. Int. J. Heat Fluid Flow 17, 89-90.

Durbin, P.A., Pettersson-Reif, B.A., 2001. Statistical theory and modeling for turbulent flows, John Willey & Sons Inc., The Atrium, Southern Gate, Chichester, West Sussex, England.

Fernandez, J.A, Elicer-Cortes, J.C., Valencia, A., Pavageau, M., Gupta, S., 2007, Comparison of low-cost two-equation turbulence models for prediction flow dynamics in twin-jets devices, Int. Commun. Heat Mass Transfer 34, 570-578.

Fröhlich, J., von Terzi, D., 2008. Hybrid LES/RANS methods for the simulation of turbulent flows, Progress in Aerospace Sciences 44, 349– 377.

Georgiadis, N.J., Yoder, D.A., Engblom, W.A., 2006. Evaluation of modified two-equation turbulence models for jet flow predictions, AIAA Journal 44, 3107-3114.

Giles, M.J., 1994a. Turbulence renormalisation group calculations using statistical mechanics methods, Physics of Fluids 6, 595-604.

Giles, M.J., 1994b. Statistical mechanics renormalisation group calculations for inhomogeneous turbulence, Physics of Fluids 6, 3750-3764.

Jaramillo, J.E., Perez-Segarra, C.D., Rodriguez, I., Oliva, A., 2008. Numerical study of plane and round impinging jets using RANS models, Numer. Heat Transfer Part B 54, 213-237.

Kok, J.C., 2000. Resolving the dependence on freestream values for the k-ω turbulence model, AIAA Journal 38, 1292-1295.

Kok, J.C., Dol, H., Oskam, H., van der Ven, H., 2004. Extra-large eddy simulation of massively separated flows, AIAA Paper 2004-0264.

Kubacki, S., Dick, E., 2009. Convective heat transfer prediction for an axisymmetric jet impinging onto a flat plate with an improved k-ω model, Int. J. Numer. Methods in Heat and Fluid Flow 19, 960-981.

Lesieur, M., 1997. Turbulence in fluids, Kluwer Academic Publishers, ISBN 0-7923-4416-2.

Magnient, J.-C., Sagaut, P., Deville, M., 2001, A study of built-in filter for some eddy viscosity models in large eddy simulation, Physics of Fluids 13, 1440-1449.

Mathey, F., Cokljat, D., Bertoglio, J.P., Sergent, E., 2006, Assessment of the vortex method for Large Eddy Simulation inlet conditions, Progress Comput. Fluid Dynamics 6, 58-67.

Maurel, S., Solliec, C., 2001. A turbulent plane jet impinging nearby and far from a flat plate, Exper. in Fluids 31, 687-696.

Menter, F.R., 1994. Two-equation eddy-viscosity turbulence models for engineering applications, AIAA Journal 32, 1598-1605.

Peng, S.H., Davidson, L., Holmberg, S., 1997. A modified low-Reynolds-number k-ω model for recirculating flows. Journal of Fluids Engineering 119, 867-875.

Piomelli, U., Radhakrishnan, S., De Prisco, G., 2008. Turbulent eddies in the RANS/LES transition region. In Advances in Hybrid RANS-LES Modeling, Eds. Peng S.-H. and Haase W., Notes on Numerical Fluid Mechanics and Multidisciplinary Design, Vol 97, Springer, ISBN 978-3-540-77813-4, 21-36.

Sagaut, P., Deck, S., Terracol, M., 2006. Multiscale and multiresolution approaches in turbulence, Imperial College Press, London.

Sakakibara, J., Hishida, K., Maeda, M., 1997. Vortex structure and heat transfer in the stagnation region of an impinging plane jet (simultaneous measurements of velocity and temperature fields by digital particle image velocimetry and laser-induced fluorescence), Int. J. Heat Mass Transfer 40, 3163-3176.

Spalart, P.R, Jou, W.-H., Strelets, M., Allmaras, S.R., 1997. Comments on the feasibility of LES for wings, and on a hybrid RANS/LES approach. In Advances in DNS/LES, Eds. Liu C. and Liu Z., Colombus O H, Greyden Press, 137-147.

Strelets, M., 2001. Detached eddy simulation of massively separated flows, AIAA Paper 2001-0879.

Tsubokura, M., Kobayashi, T., Taniguchi, N., Jones, W.P., 2003. A numerical study on the eddy structures of impinging jets exited at the inlet, Int. J. Heat Fluid Flow 24, 500-511.

Tu, C.V., Wood, D.H., 1996. Wall pressure and shear stress measurements beneath an impinging jet, Experimental Thermal and Fluid Sci. 13, 364-373.

Wilcox, D.C., 1998, Turbulence modeling for CFD, 2-nd ed., DCW Industries, Inc., La Canada, CA.

Wilcox, D.C., 2008. Formulation of the k-ω turbulence model revisited, AIAA Journal 46, 2823-2837.

Yan, J., Mocket, C., Thiele, F., 2005, Investigation of alternative length scale substitutions in detached-eddy simulation, Flow, Turbulence and Combustion 74, 85-102.

Yoshizawa, A., 1993. Bridging between eddy-viscosity-type and second-order turbulence models through a two-scale turbulence theory, Physical Review E 48, 273-281.

Zhe, J., Modi, V., 2001. Near wall measurements for a turbulent impinging slot jet, Trans. of the ASME, J. Fluid Eng. 123, 112-120.

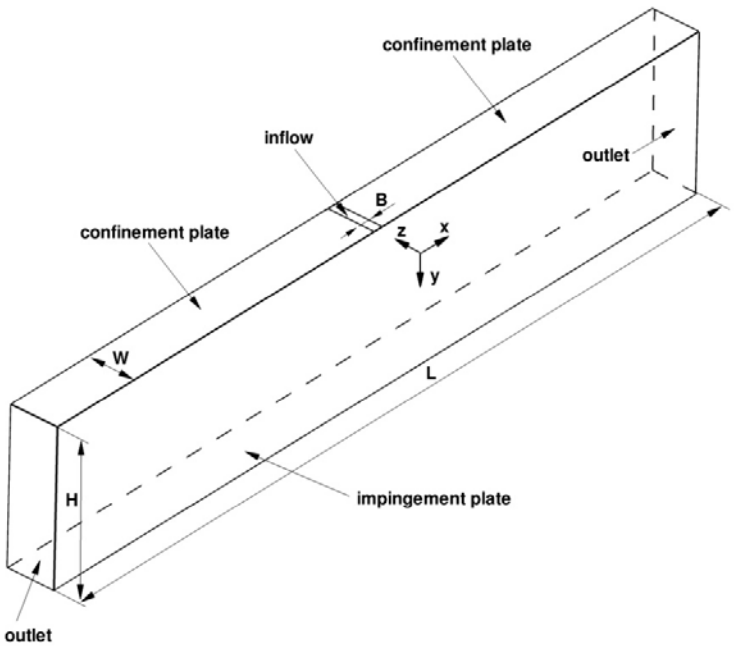

Figure 1: Scheme of the computational domain.

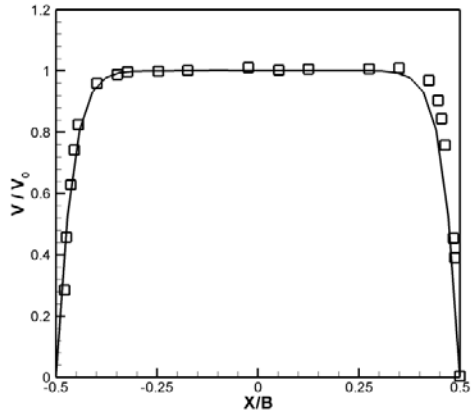

Figure 2: Profile of the mean v-velocity component imposed at the nozzle exit. Comparison with the experiments of Maurel and Solliec (2001).

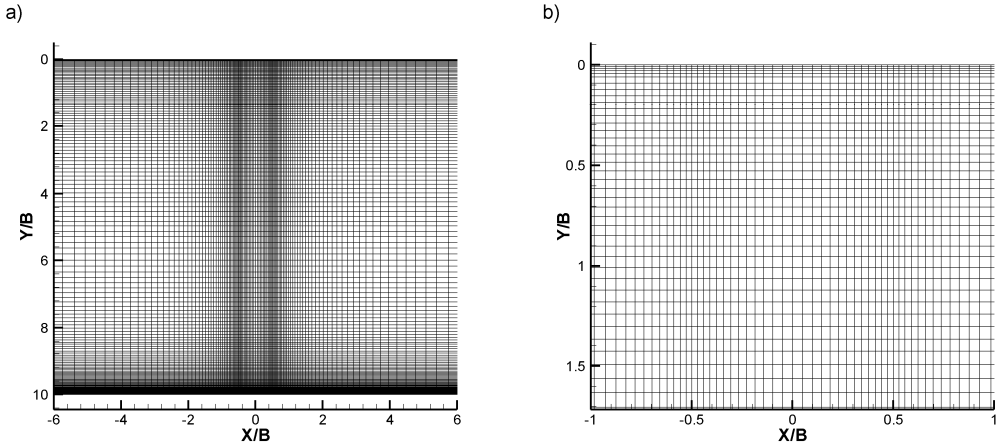

Figure 3: (a) Computational mesh in the x-y plane at distance |X/B|<6 and (b) close-up view in vicinity of the nozzle exit (|X/B|<0.5, Y/B=0) for H/B=10 and Re=13500 (basic mesh).

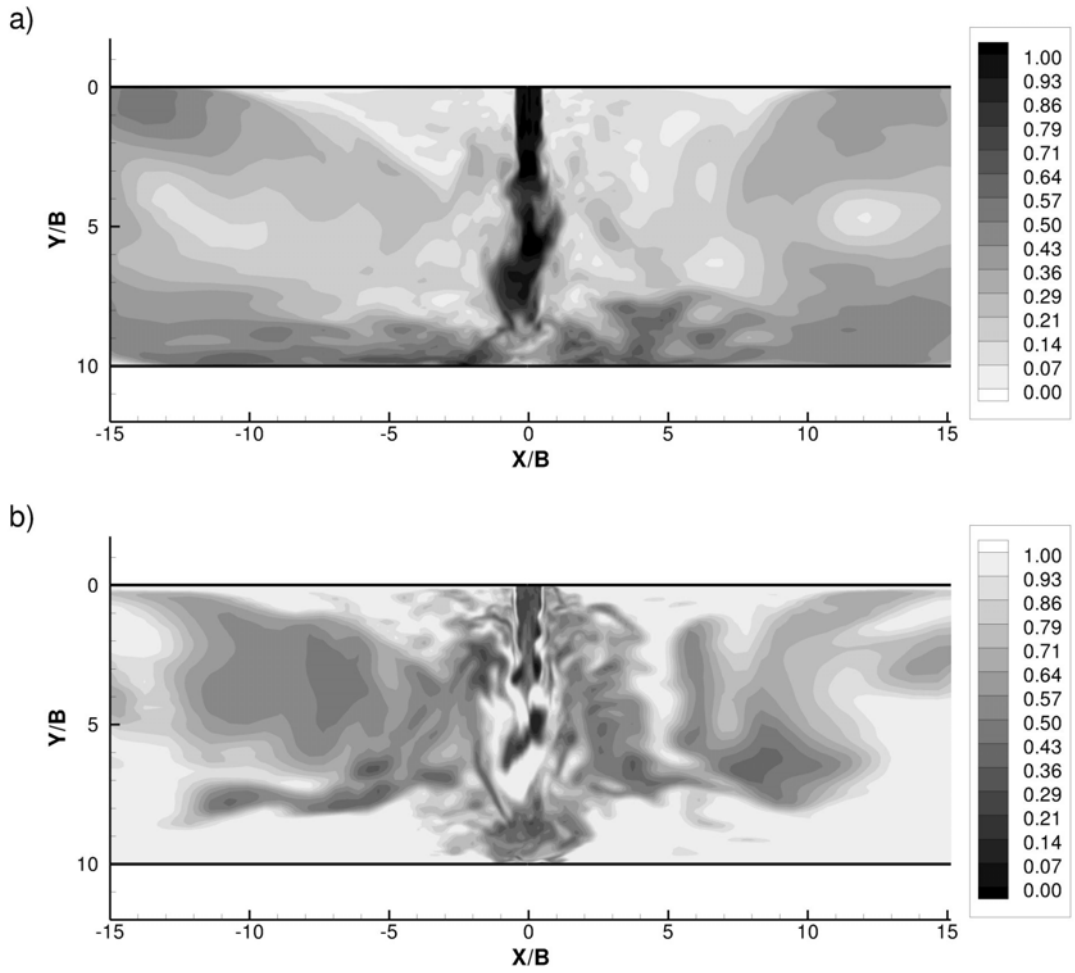

Figure 4: Contour plots of (a) instantaneous velocity magnitude, V_{magn}/V_0 and (b) instantaneous field of $f = min(1, C_{DES}\Delta/L_t)$ ($f < 1$: LES region, $f = 1$: RANS region) in the x-y plane ($z/B = \pi/2$) for H/B=10, Re=13500 obtained with model M2.

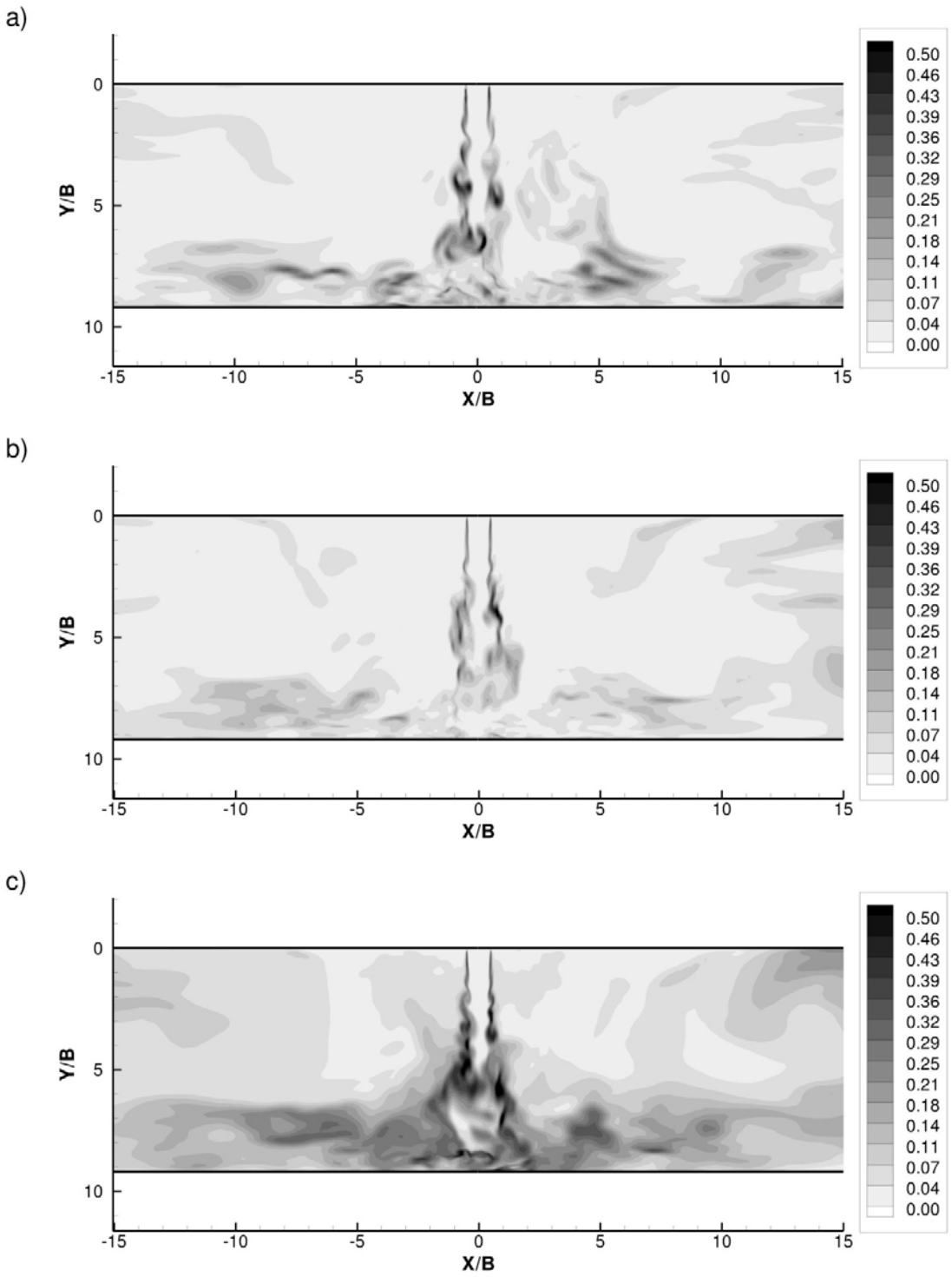

Figure 5: Instantaneous field of modelled turbulent kinetic energy, k/V_0^2 obtained by (a) M1-model (b) M2-model and (c) M3-model, for *H/B*=9.2, *Re*=20000.

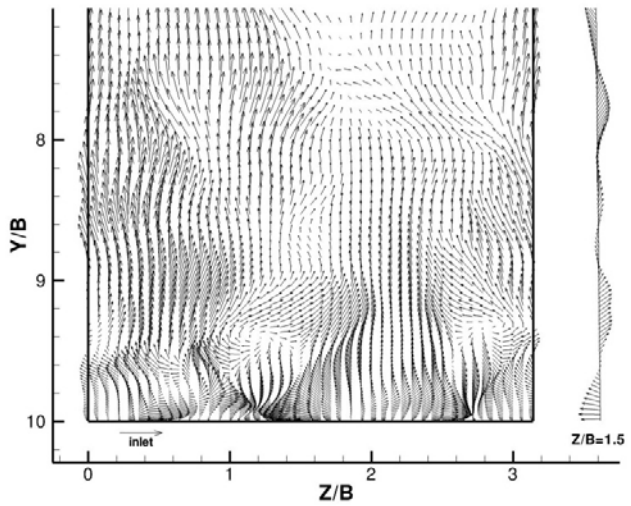

Figure 6: Counter-rotating vortices close to the impingement plate in the z-y plane at distance *X/B*=-0.5 for *H/B*=10, *Re*=13500 with the M2 model (normalized velocity vectors in the z-y plane). The cut on the right (*Z/B*=1.5) shows the strength of the vortices in the x-direction. For comparison, the length of the unit velocity vector at the jet exit (denoted by 'inlet') is shown close to the bottom wall (Y/B=10).

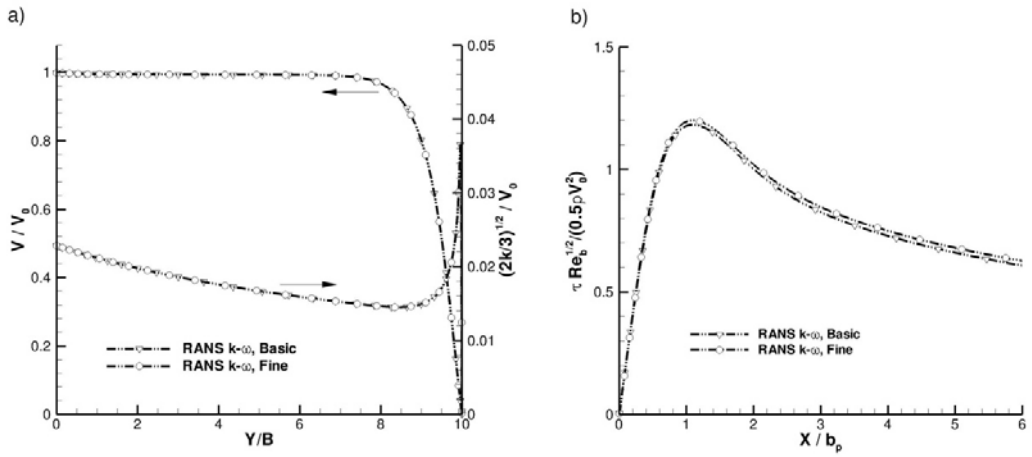

Figure 7: Influence of the grid density on the RANS results: a) evolution of mean and fluctuating y-velocity in the symmetry plane; b) skin friction coefficient along the impingement plate; for H/B=10, Re=13500.

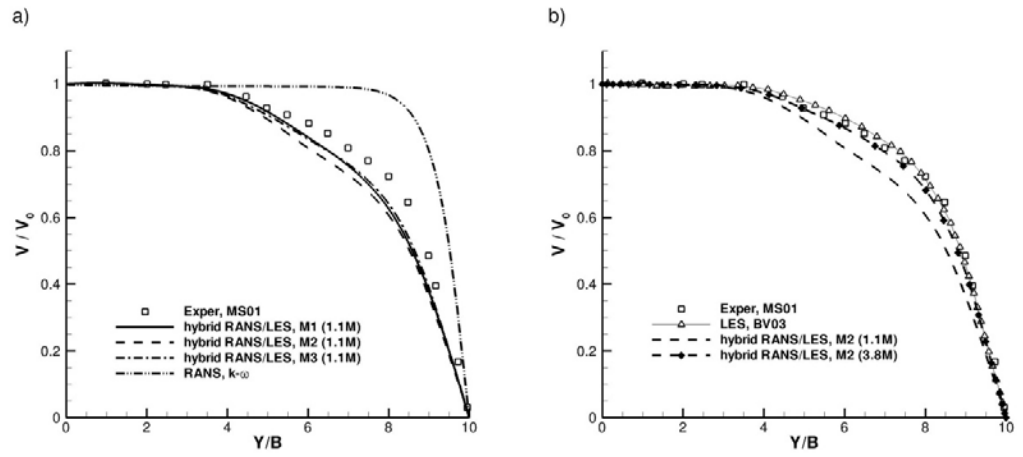

Figure 8: Evolution of mean y-velocity in the symmetry plane for H/B=10, Re=13500.

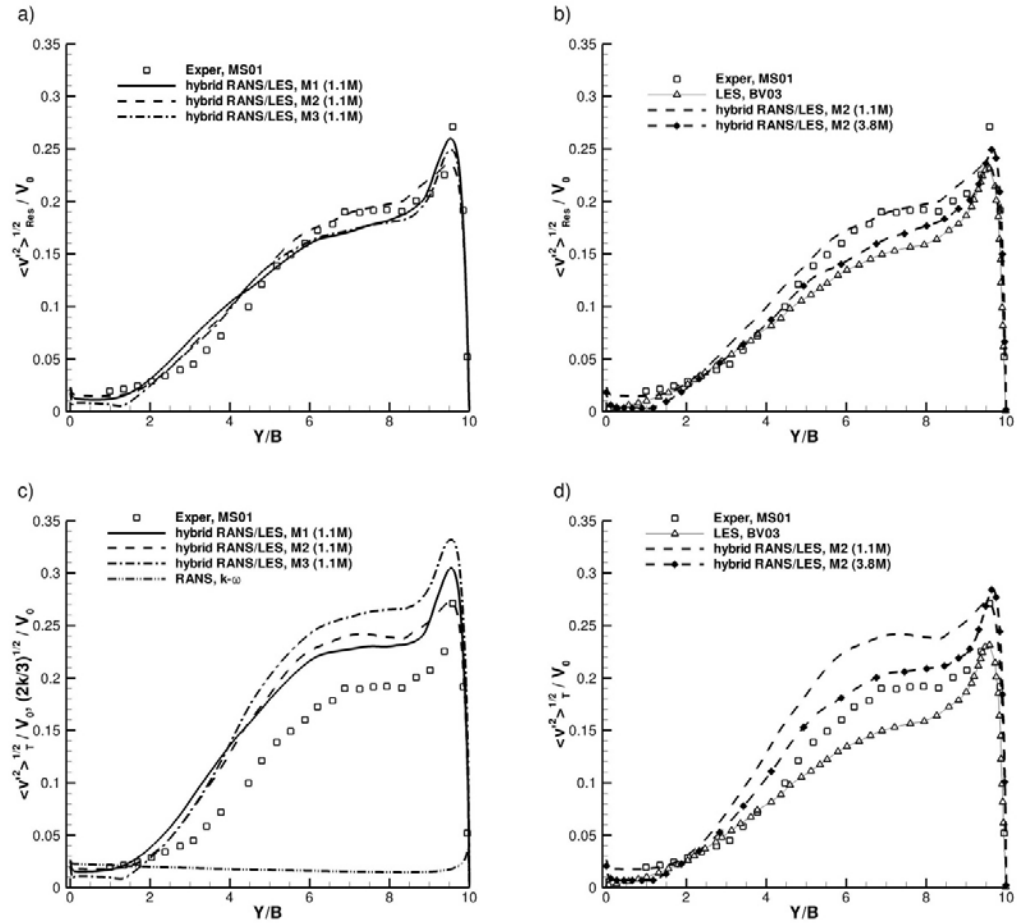

Figure 9: Evolution of fluctuating y-velocity in the symmetry plane for H/B=10, Re=13500. For hybrid RANS/LES computations: (a,b) resolved and (c,d) total fluctuating velocities. For LES, only resolved fluctuations are shown.

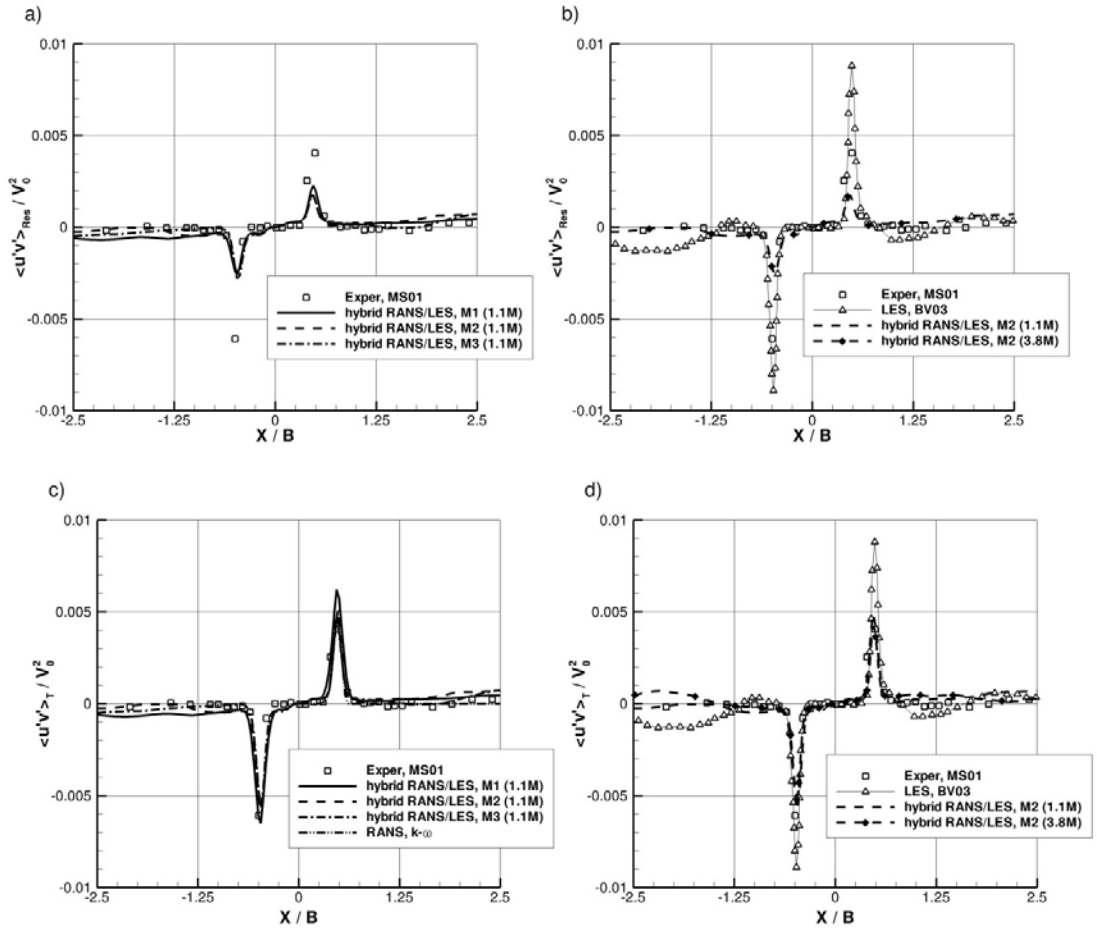

Figure 10: Profiles of (a,b) resolved and (c,d) total Reynolds stress $\langle u'v' \rangle / (V_0)^2$ along *X/B* at distance *Y/H*=1/12 from the jet exit for *H/B*=10, Re=13500. For LES, only resolved fluctuations are shown

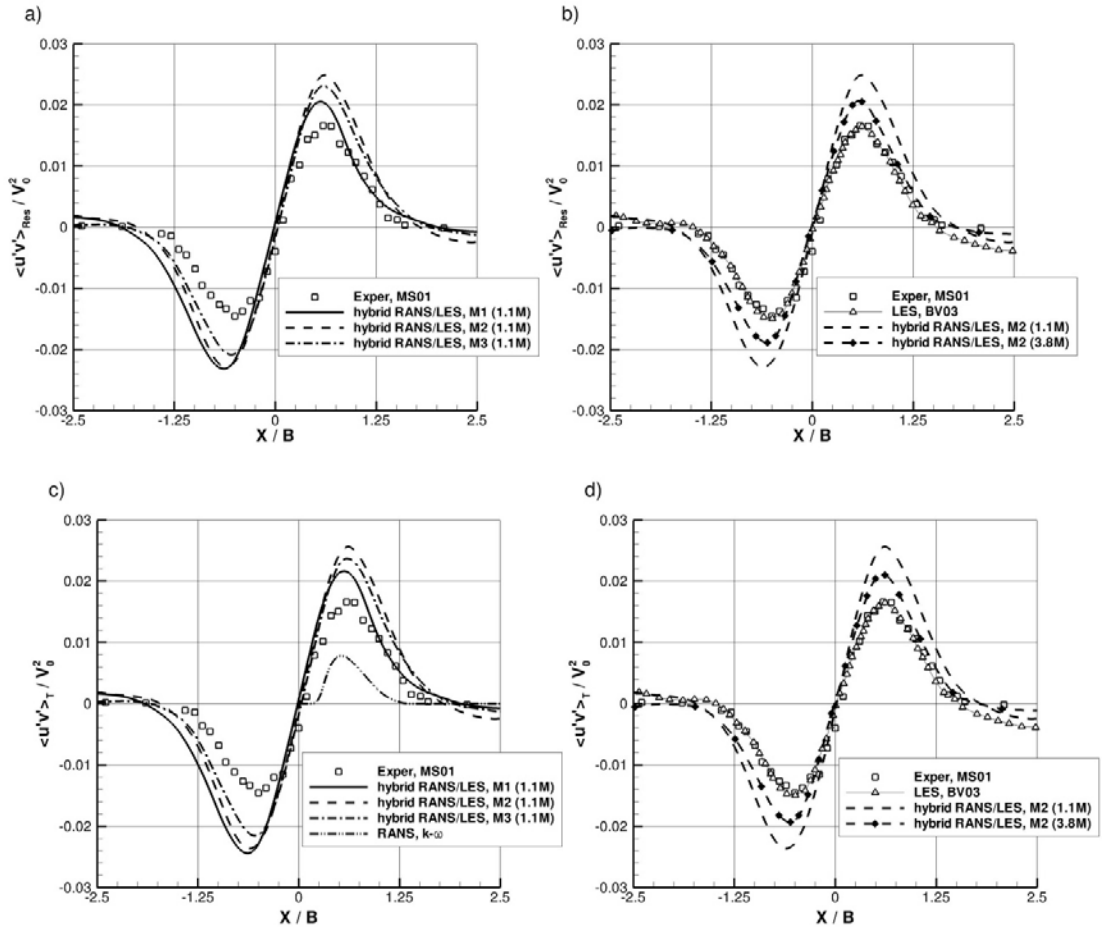

Figure 11: Profiles of (a,b) resolved and (c,d) total Reynolds stress $\langle u'v' \rangle/(V_0)^2$ along *X/B* at distance *Y/H*=0.5 from the jet exit, for *H/B*=10, Re=13500. For LES, only resolved fluctuations are shown

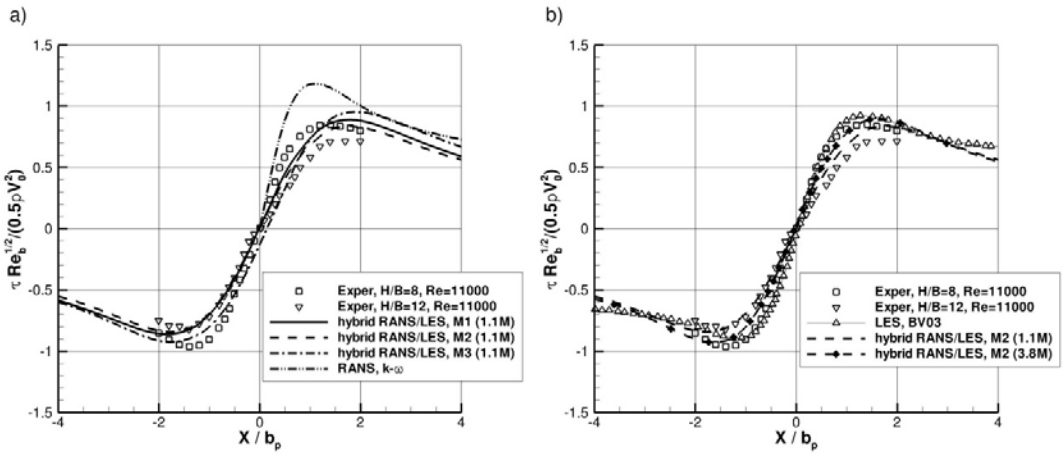

Figure 12: Distribution of $\tau \,\mathrm{Re}_b^{1/2} / \left(0.5 \rho V_0^2\right)$ along the impingement plate (distance x is normalized by half-width b_p of the impingement pressure profile, (Tu and Wood, 1996)) for *H/B*=10, *Re*=13500.

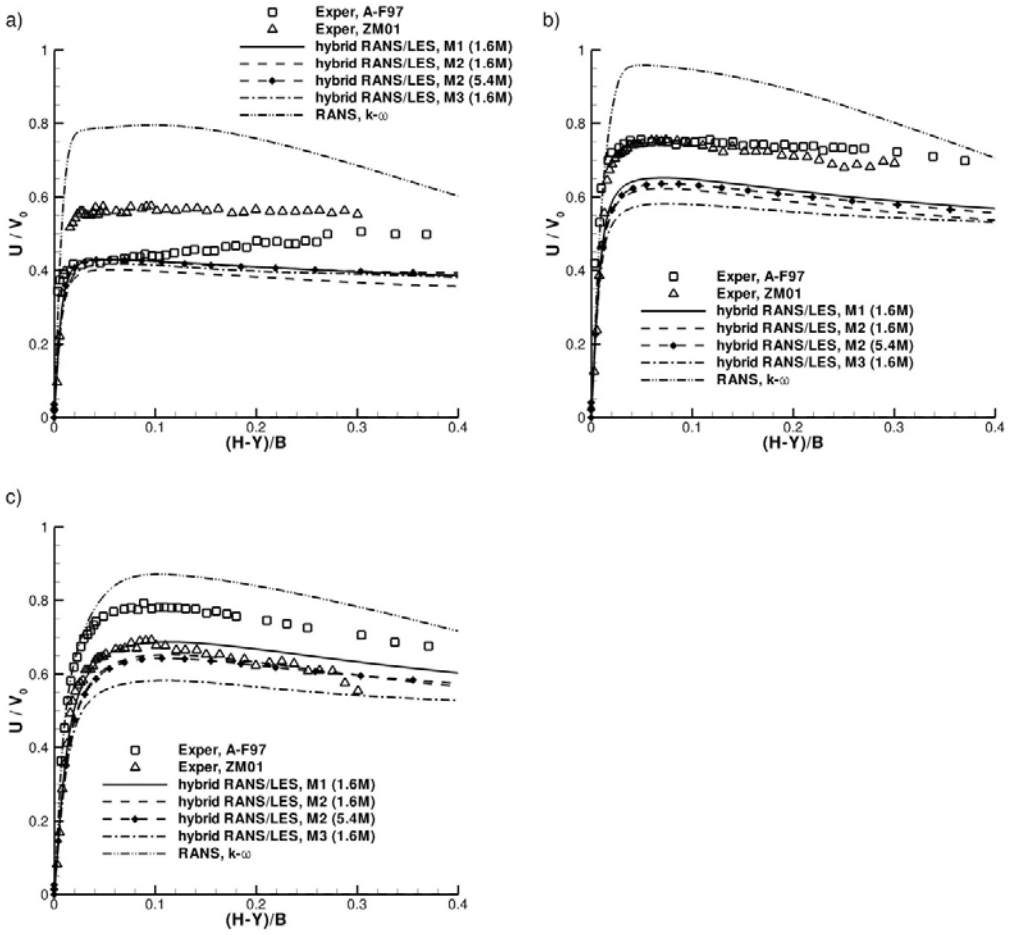

Figure 13: Variation of the mean x-velocity component along a line perpendicular to the impingement plate at different positions from the symmetry plane a) *x/B*=1, b). *x/B*=2, c) *x/B*=5 for *H/B*=9.2, *Re*=20000.

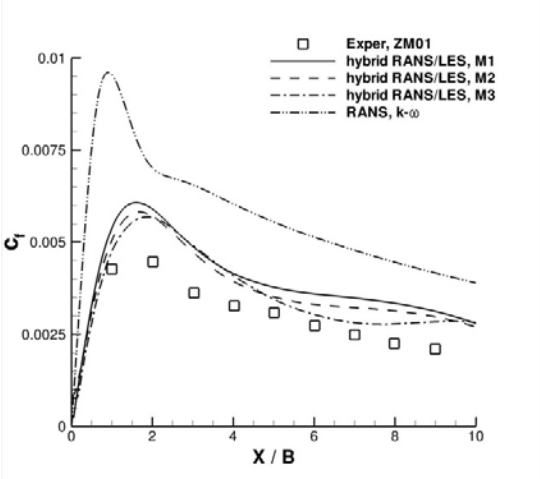

Figure 14: Distribution of the skin friction coefficient along the impingement plate for *H/B*=9.2, *Re*=20000.

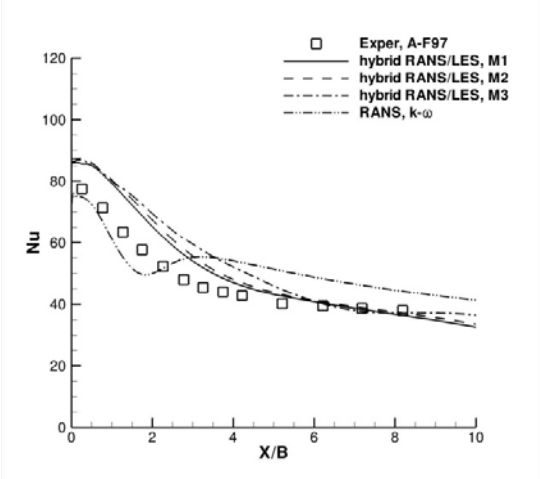

Figure 15: Distribution of the Nusselt number along the impingement plate for *H/B*=9.2, *Re*=20000.

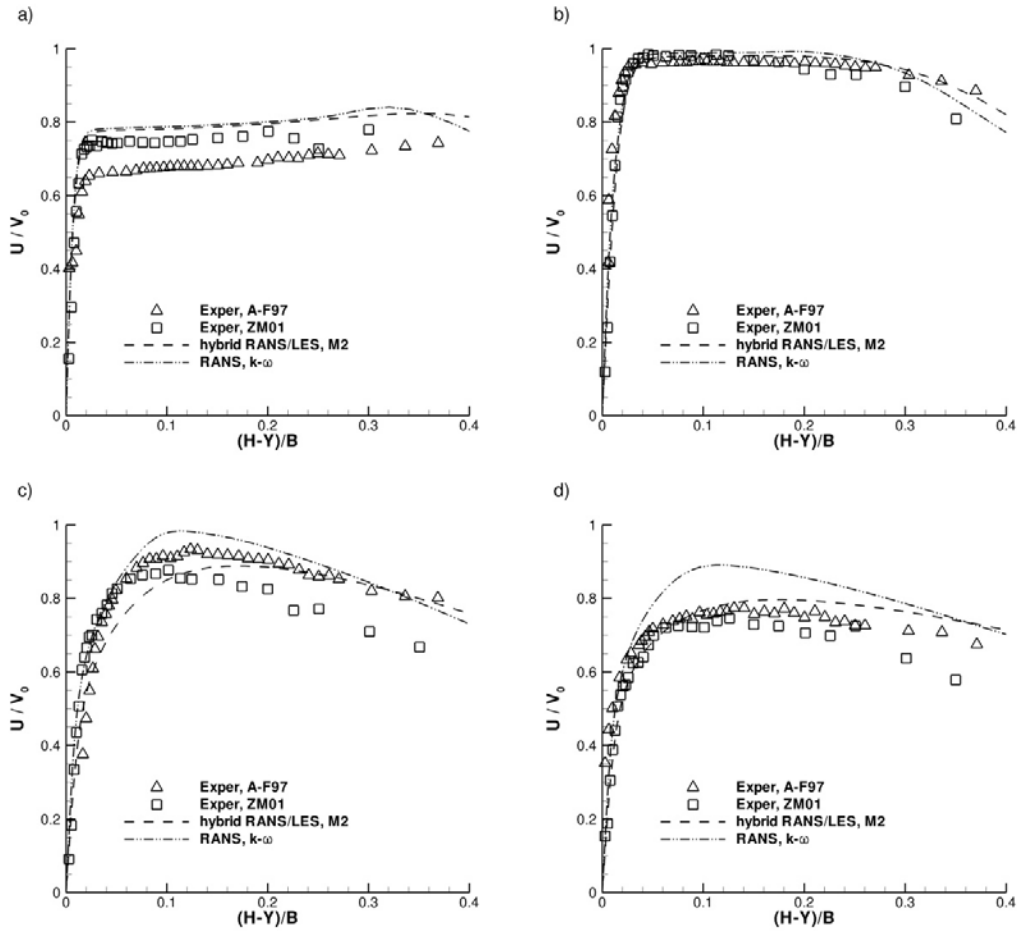

Figure 16: Variation of the mean x-velocity component along a line perpendicular to the impingement plate at different positions from the symmetry plane a) *x/B*=1, b). *x/B*=2, c) *x/B*=5, d) *x/B*=7 for *H/B*=4, *Re*=20000.

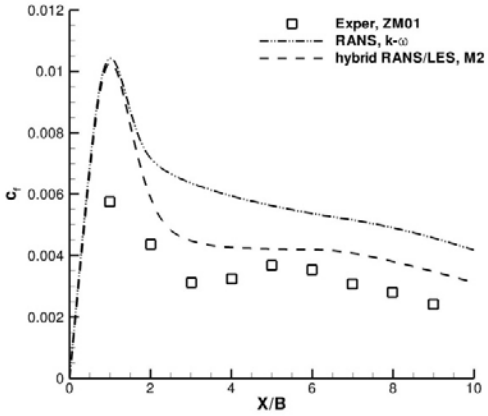

Figure 17: Distribution of the skin friction coefficient along the impingement plate for *H/B*=4, *Re*=20000.

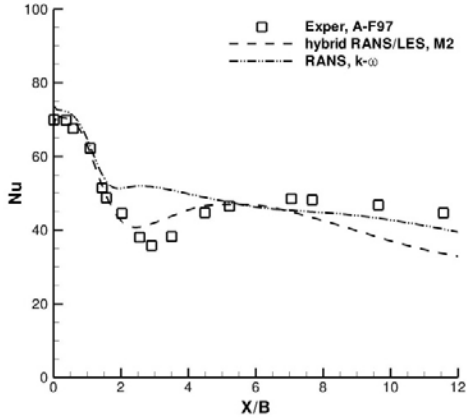

Figure 18: Distribution of the Nusselt number along the impingement plate for *H/B*=4, *Re*=20000.

Table 1: Dissipation term D_k and turbulent viscosity ν_t for models M1, M2 and M3. $L_t = k^{1/2}/\beta^* \omega$

Model	D_k	ν_t
M1	$\beta^* k\omega \max(1, L_t/C_{DES}\Delta)$	k/ω
M2	$\beta^* k\omega \max(1, L_t/C_{DES}\Delta)$	$k/\omega \min(1, C_{DES}\Delta/L_t)$
M3	$\beta^* k\omega$	$k/\omega \min(1,(C_{DES}\Delta/L_t)^{4/3})$

Table 2: Equilibrium conditions for the hybrid RANS/LES models and values of the Smagorinsky constant in LES mode under equilibrium conditions.
$P_k=\nu_t S^2$, D_k is defined in Table 1, $P_\omega=\alpha S^2$ and $D_\omega=\beta\omega^2$.

model	*Equilibrium conditions*	*Smagorinsky coefficient C_s ($\nu_t=(C_s\Delta)^2 S$)*	*Value of C_s*
M1	$P_k=D_k$, $P_\omega=D_\omega$	$(\beta/\alpha)^{3/4} C_{DES}$	*0.13 for β=0.06* *0.15 for β=0.0708*
M2	$P_k=D_k$	$(\beta^*)^{3/4} C_{DES}$	*0.11*
M3	$P_k=D_k$	$(\beta^*)^{3/4} C_{DES}$	*0.11*

Table 3: Length L, height H and width W of the computational domains for simulations performed with the hybrid RANS/LES models and the number of cells N_x, N_y, N_z in x, y and z directions.

Case	*L/B*	*H/B*	*W/B*	N_x	N_y	N_z
H/B=10, *Re*=13500 (Basic)	80	10	π	170	150	44
H/B=10, *Re*=13500 (Fine)	80	10	π	260	225	66
H/B=9.2, *Re*=20000 (Basic)	80	9.2	π	220	165	44
H/B=9.2, *Re*=20000 (Fine)	80	9.2	π	330	248	66
H/B=4, *Re*=20000	80	4	π	220	90	44